Journal of Chromatography B, 875 (2008) 180–191

Contents lists available at ScienceDirect

Journal of Chromatography B

journal homepage: www.elsevier.com/locate/chromb

On-column epimerization of dihydroartemisinin: An effective analytical approach to overcome the shortcomings of the International Pharmacopoeia monograph☆

Walter Cabri[a], Alessia Ciogli[b], Ilaria D'Acquarica[b], Michela Di Mattia[a], Bruno Galletti[a], Francesco Gasparrini[b,*], Fabrizio Giorgi[a], Silvana Lalli[a], Marco Pierini[b], Patrizia Simone[b]

[a] Analytical Development, R&D Department, sigma-tau S.p.A., Via Pontina km 30,400, 00040 Pomezia, Italy
[b] Dipartimento di Chimica e Tecnologie del Farmaco, Sapienza Università di Roma, P. le Aldo Moro 5, 00185 Rome, Italy

ARTICLE INFO

Article history:
Received 11 April 2008
Accepted 20 June 2008
Available online 27 June 2008

Keywords:
Dihydroartemisinin (DHA)
Antimalarials
Epimerization study
Cryo-HPLC
Dynamic HPLC (DHPLC)
Computer simulation

ABSTRACT

We developed a cryo-HPLC/UV method for the simultaneous determination of artemisinin (**1**), α-dihydroartemisinin (**2**α), β-dihydroartemisinin (**2**β), and a ubiquitous thermal decomposition product of **2** (designated as diketoaldehyde, **3**), starting from the International Pharmacopoeia monograph on dihydroartemisinin. The method takes for the first time the on-column epimerization process of **2** into consideration. Chromatographic separation was obtained under reversed-phase conditions on a Symmetry C18 column (3.5 μm particle size) with a mobile phase consisting of acetonitrile–water 60:40 (v/v), delivered at 0.60–1.00 ml/min flow-rates, with ultraviolet detection at low wavelength (λ = 210 nm). Low temperatures (T = 0–10 °C) were selected on the grounds of a diastereoselective dynamic HPLC (DHPLC) study performed at different temperatures, aimed at identifying the best experimental conditions capable of minimizing the on-column interconversion process.

1. Introduction

Artemisinin (**1**, Fig. 1) is a sesquiterpene lactone endoperoxide isolated from *Artemisia annua* L. that Chinese herbalists traditionally use to treat malaria [1]. Since its identification in the 1970s, artemisinin, as well as semi-synthetic derivatives [2] and synthetic trioxanes [3], have been used in therapy. Reduction of artemisinin by sodium borohydride [4] produced dihydroartemisinin (DHA, **2**, Fig. 1), which is also its main metabolite and provides improved antimalarial potency and a major elimination route [3]. The synthesis of **2** opened pathways for further derivatization at C-10 to give ether and ester derivatives, largely exploited by the Chinese [5] with the aim of tuning water and/or oil solubility and improving bioavailability. The conversion of the lactone carbonyl group at C-10 of **1** into the hydroxyl (hemiacetal) group in **2** yields a new sterically labile centre in the molecule, which, in turn, provides two lactol hemiacetal epimers, namely, **2**α and **2**β (Fig. 2A). The α-epimer bears the hydroxyl group in the equatorial position (absolute stereochemistry at C-10: *R*), whereas the β-epimer possesses an axial hydroxyl group [6]. Although **2** has a chair-like pyranose ring, such nomenclature is the reverse of that normally used for designating the stereochemistry of sugars and glycosides, in which, for example, α-D-glucopyranose possesses an axial hydroxyl group [7].

Bulk crystalline **2** is the **2**β-epimer (see Fig. 2B), as illustrated by an X-ray crystallographic study on crystals of **2** [8]. Dissolution of vacuum-dried solid **2** in $CDCl_3$ provides a solution consisting exclusively of **2**β, which equilibrates to a 1:1 mixture of **2**α and **2**β within 10 h [8,9]. The rate and extent of interconversion of the epimers in solution was shown to be dependent on solvent polarity [9,10].

Numerous HPLC methods were developed for the analysis and plasma levels monitoring of **2**, formerly based on two main detection strategies: reductive electrochemical (EC) [11–17] and UV detection [18–20] involving pre- or post-column derivatization. The latter approach lacks specificity in that metabolites of the drug are also converted, in many instances, to identical UV-absorbing products. On the other hand, HPLC-EC provides excellent specificity and sensitivity, although it suffers from some inherent difficulties, i.e., rigorous deoxygenation of samples and mobile phases, and special laboratory facilities are needed. To overcome these shortcomings, evaporative light scattering detection (ELSD) was coupled for the first time to the HPLC analysis of artemisinin and related analogues

☆ This paper is part of the special issue 'Enantioseparations', dedicated to W. Lindner, edited by B. Chankvetadze and E. Francotte.

* Corresponding author. Tel.: +39 06 49912776; fax: +39 06 49912780.
E-mail address: francesco.gasparrini@uniroma1.it (F. Gasparrini).

1570-0232/$ – see front matter © 2008 Elsevier B.V. All rights reserved.
doi:10.1016/j.jchromb.2008.06.037

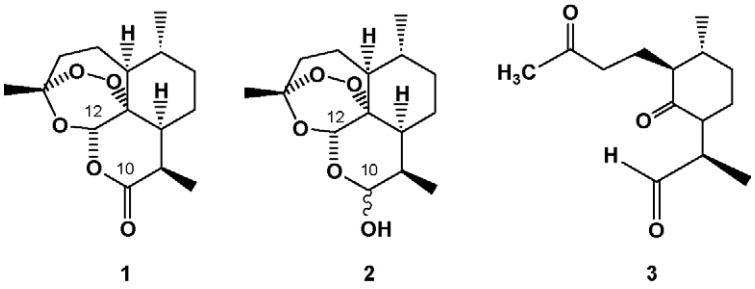

Fig. 1. Chemical structures of artemisinin (**1**), dihydroartemisinin (DHA, **2**), and a thermal decomposition product of dihydroartemisinin, designated as diketoaldehyde (DKA, **3**).

[21]. The high sensitivity and selectivity of mass spectrometry (MS) opened the way to a large production of analytical methods based on the HPLC-MS coupling [22–26] for the plasma monitoring of **2**, either based on atmospheric pressure chemical ionization (APCI) [23,26] or electrospray ionization (ESI) mode [22,24,25]. Radiochromatographic detection [27] was exploited as well in a recent HPLC study aimed at determining the **2**α/**2**β ratio in vivo and evaluating the protein binding of **2**. Notwithstanding such large availability in the literature of robust HPLC methods suitable for the analysis of **2**, only a few were designed for the differential quantitation of the two isomeric forms of **2** [15,16,18,19,26,27]. As a result, efficient and robust separation of the two interconverting species must be a prerequisite of any analytical method aimed at quantitating the drug in active ingredient, pharmaceutical formulations, and biological fluids. Moreover, since previous studies [28,29] on the equilibrium between **2**α and **2**β showed that interconversion of the two epimers occurred in a chromatographic time scale, an ideal HPLC analytical method for **2** should prevent the epimerization phenomena during the separation process and allow quantification of the two epimers even in the presence of related substances. For example, a pharmaceutical batch of **2** can contain several impurities arising from the specific synthetic procedure [4], such as the starting material itself (i.e., **1**), and a thermal decomposition product, designated as diketoaldehyde (DKA, **3**, Fig. 1) [30,31]. In the present paper we describe the development of an HPLC/UV method for the simultaneous determination of **1**, **2**α, **2**β, and **3**, which, for the first time, takes into consideration the on-column epimerization process of **2**. Starting from the International Pharmacopoeia monograph on dihydroartemisinin [32], we identified some optimal conditions (such as stationary phase and column temperature) to minimize on-column epimerization while achieving the best selectivity and efficiency of separation. In another related paper, we will evaluate the influence of mobile phase composition to both improve the overall selectivity and minimize the on-column interconversion.

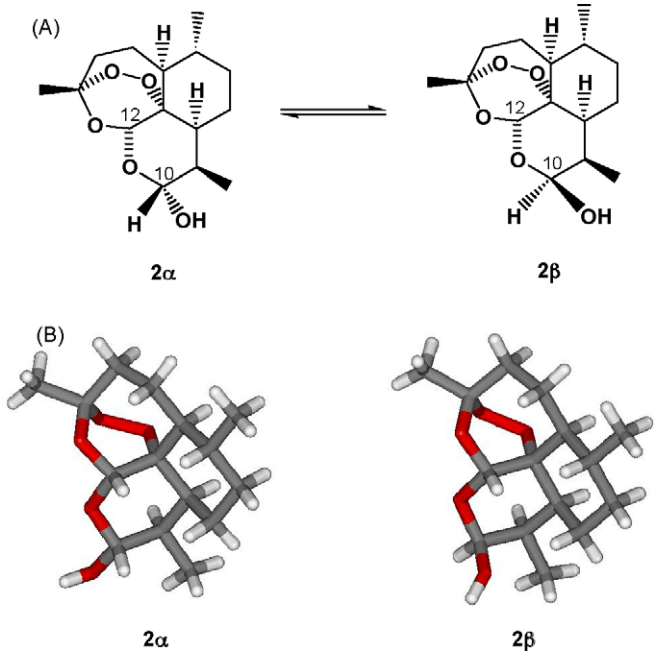

Fig. 2. Chemical structure (A) and polytube model (B) of the interconverting epimers of dihydroartemisinin: the **2**α-epimer bears the hydroxyl group in the equatorial position (absolute stereochemistry at C-10: *R*), whereas the **2**β-epimer possesses an axial hydroxyl group. Polytube model of the **2**β-epimer was obtained by computer editing of the X-ray data of crystalline **2**β [8]; the model for the **2**α-epimer was derived by molecular mechanics optimization (MMFF force field as implemented in SPARTAN'04 1,0,0) by inverting the configuration at C-10.

2. Experimental

2.1. Apparatus

Liquid chromatography was performed using a Waters Model 2695 HPLC separation module (Waters, Milford, MA, USA) coupled with a Waters 996 Photodiode Array Detector. Chromatographic data were collected and processed using Empower2 software (Waters).

Variable temperature HPLC was performed by using a thermally insulated container cooled by the expansion of liquid carbon dioxide (CO_2). Flow of liquid CO_2 and column temperature were regulated by a solenoid valve, thermocouple, and electric controller. Temperature variations after thermal equilibration were within ±0.1 °C.

^{1}H-NMR spectra were recorded at T = 25 °C on a Varian INOVA 500 MHz spectrometer equipped with a triple resonance indirect probe (TRIAX). Data acquisition, Fourier transformation, and spectra elaboration were performed using the Varian software VNMR, 6.1C.

2.2. Chemicals and reagents

Artemisinin (**1**), dihydroartemisinin (DHA, **2**), and diketoaldehyde (DKA, **3**) samples were supplied by sigma-tau S.p.A., Pomezia (Italy). HPLC-grade acetonitrile, methanol, and water were purchased from Carlo Erba (Italy). HPLC-grade acetonitrile from Merck (Darmstadt, Germany) was also tested. Deuterium oxide was from Sigma–Aldrich (St. Louis, MO, USA). The following commercially available reversed-phase C18 HPLC columns were used: Zorbax SB-C18 (Agilent Technologies, Santa Clara, CA, USA); Luna C18 (Phenomenex, Inc., Torrance, CA, USA); YMC-Pack *Pro*C18 RS (YMC Europe GmbH, Dinslaken, Germany); SunFire C18 (Waters); Symmetry C18 (Waters); Gemini C18 (Phenomenex, Inc.); Acclaim 120 C18 (Dionex Corporation, Sunnyvale, CA, USA); Ascentis Express

Table 1
Physicochemical data of the tested commercial RP-C18 columns

Column	Dimension (mm × mm)	Particle size (μm)	Pore size (Å)	Surface area ($m^2\ g^{-1}$)	End-capped	$K_0 \times 10^{14}$ (m^2)	Carbon load		Hold-up time[a] (min)
							(%)	(μmol m^{-2})	
Zorbax SB-C18	150 × 4.6	5.0	80	180	No	4.41	–	2.00	1.56
Luna C18	150 × 4.6	5.0	100	440	Yes	2.51	19.00	3.00	1.70
YMC-Pack *Pro*C18 RS	150 × 4.6	5.0	80	500	Yes	2.36	21.90	–	1.61
SunFire C18	150 × 4.6	3.5	96	331	Yes	1.31	16.62	3.76	1.63
Symmetry C18[b]	150 × 4.6	3.5	100	340	Yes	1.70	19.67	3.15	1.56
Gemini C18	150 × 4.6	3.0	110	375	Yes	1.30	14.00	–	1.78
Acclaim 120 C18	150 × 4.6	3.0	120	300	Yes	1.56	18.00	3.20	1.79
Ascentis Express C18	150 × 4.6	2.7	90	150	Yes	1.18	–	3.50	1.45
Chromolith RP-18	100 × 4.6	–	–	300	Yes	5.95	18.00	3.60	1.54

[a] Mean value of 3 injections (sample: nitromethane; eluent: acetonitrile; flow-rate: 1.00 ml/min; T = 25 °C; UV detection at 254 nm).
[b] Also checked in different column lengths (100 mm × 4.6 mm and 75 mm × 4.6 mm I.D.)

C18 (Sigma–Aldrich); Chromolith RP-18 (Merck). Details of the columns are collected in Table 1.

2.3. Chromatographic procedures

2.3.1. Room temperature chromatography

Chromatographic separations were obtained under reversed-phase conditions with a mobile phase consisting of acetonitrile–water 60:40 (v/v), delivered at a flow-rate of 1.00 ml/min, with ultraviolet detection at 210 nm.

Columns temperature was set at T = 25 °C. Columns hold-up time (t_0) was determined from the elution time of an unretained marker (nitromethane) using acetonitrile as eluent, at T = 25 °C, flow-rate 1.00 ml/min and UV detection at 254 nm. Hold-up times, obtained as mean value of 3 injections, are reported in Table 1.

2.3.2. Variable temperature chromatography

Variable temperature HPLC was performed by placing the columns inside the device described in Section 2.1. Chromatographic conditions were as reported in Section 2.3.1, except for column temperature.

2.3.3. Low-temperature chromatography

Low-temperature separations were performed merely on the Symmetry C18 column, tested in three different column lengths, i.e., 150, 100, and 75 mm × 4.6 mm I.D. Chromatographic conditions were acetonitrile–water 60:40 (v/v), flow-rate 0.60 ml/min (0.60–2.0 ml/min for geometry 75 mm × 4.6 mm I.D.), and UV detection at 210 nm. Columns temperature was set at T = 0, 5, and 10 °C.

2.4. Sample preparation

Approximately 10 mg, accurately weighed, of a bulk sample of **2** were transferred into a 10 ml glass volumetric flask and then approximately 10 ml of mobile phase was added. The mixture was sonicated to dissolve, diluted to volume with mobile phase, and allowed to equilibrate at T = 25 °C (**2**α/**2**β ratio of about 3.2). A separate solution of **1** was prepared as follows: approximately 10 mg, accurately weighed, of **1** were transferred into a 5 ml glass volumetric flask and then approximately 5 ml of mobile phase was added. The mixture was sonicated to dissolve and diluted to volume with mobile phase. The final concentration of the above solutions was about 1 mg/ml for **2** and 2 mg/ml for **1**. A 200 μl aliquot of the latter solution was added to the former, and a 5 μl aliquot of the final mixture was injected into the HPLC system. Compound **3** is a thermal decomposition impurity which is formed after prolonged storage of **2** [31] and thus always present in small amounts upon dissolution of **2**. For the variable temperature HPLC experiments (see Section 2.3.2), a purified sample of **2**, recrystallized from ethanol, was also employed, and dissolved in mobile phase as described above.

2.5. ^{1}H-NMR calculation of the thermodynamic ratio ($K_{\alpha/\beta}$)

A 1 mg/ml solution of a purified sample of **2**, recrystallized from ethanol, was prepared in mobile phase, and sonicated to dissolve. A 0.05 ml aliquot of D_2O was added to 0.6 ml of the above solution, and the mixture was allowed to equilibrate at T = 25 °C. The final solvent composition was acetonitrile–water 55.4:44.6 (v/v). ^{1}H-NMR spectra were acquired by means of the DPFGSE solvent suppression sequence [33], in which the selective pulses were convoluted to obtain simultaneous suppression of the non-deuterated solvents. 64 scans were acquired, with a recycle delay of 3 s, and three independent spectra were acquired. From integration of the singlets at δ = 5.55 and 5.40 ppm, corresponding to the protons at C-12 for **2**β and **2**α epimers respectively (see Fig. 1), the **2**α isomer was 78.6 ± 0.3% ($^{\text{H-NMR}}K_{\alpha/\beta}$ = 3.5). The very same sample was processed under optimized cryo-HPLC conditions (*vide infra*), giving a 77.8 ± 0.2% value ($^{\text{HPLC}}K_{\alpha/\beta}$ = 3.5) for the same isomer.

2.6. Simulation of diastereoselective dynamic chromatograms

Simulation of variable-temperature experimental chromatograms was performed by using the lab-made computer program Auto DHPLC y2k [34] which implements both stochastic and theoretical plate models according to mathematical equations and procedures described within ref. [35a,b], respectively. A quite comprehensive view of milestone works on dynamic chromatography and its applications is given in ref. [36]. The developed algorithm may take into account all types of first-order interconversions, i.e. enantiomerizations as well as diastereomerizations or constitutional isomerizations, (e.g. pseudo first-order tautomerizations). Within non-enantiomeric isomerizations, forward and backward interconversion occur at different rates in the achiral mobile phase, where the two isomerizing species are present in differing amounts. According to the thermodynamic cycle involved inside a virtual chromatographic theoretical plate for a generic first-order isomerization process concomitant with the chromatographic repartition equilibria (see Chart 1), we applied in the algorithm the following general equation:

$$\frac{k^{\text{m}}_{-1}}{k^{\text{m}}_{1}} \times \frac{k^{\text{s}}_{1}}{k^{\text{s}}_{-1}} = \frac{k'_{\text{B}}}{k'_{\text{A}}}$$

where k'_{A} and k'_{B} are the retention factors of the first (A) and second (B) eluting species, k^{m}_{-1} and k^{m}_{1} are the rate constants for the backward and forward interconversion in mobile phase, respectively, and k^{s}_{1} and k^{s}_{-1} are the rate constants for the forward and backward interconversion in stationary phase, respectively.

$$K_D^A = \frac{\phi}{k'_A} \quad ; \quad K_D^B = \frac{\phi}{k'_B}$$

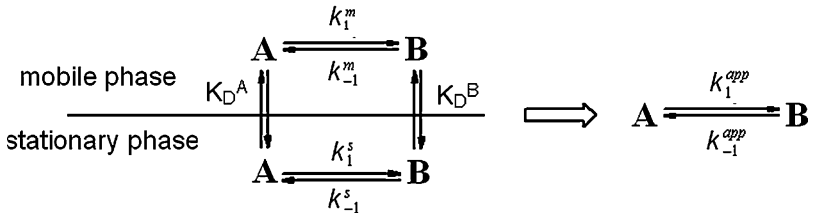

Chart 1.

Program functionality was validated on several first-order isomerizations (both enantiomerization and non-enantiomerization) by comparing DHPLC results with those obtained by DNMR technique [34a–d] or by classical method [34e]. The algorithm also implements the chance of taking tailing effects into account. Both chromatographic and kinetic parameters can be automatically optimized by simplex algorithm until obtaining the best agreement between experimental and simulated dynamic chromatograms. In the present paper all simulations were performed employing the stochastic model and taking tailing effects into consideration.

3. Results and discussion

3.1. Pharmacopoeia guidelines on antimalarial drugs

Initially, we decided to start our investigation by referring to the International Pharmacopoeia guidelines on

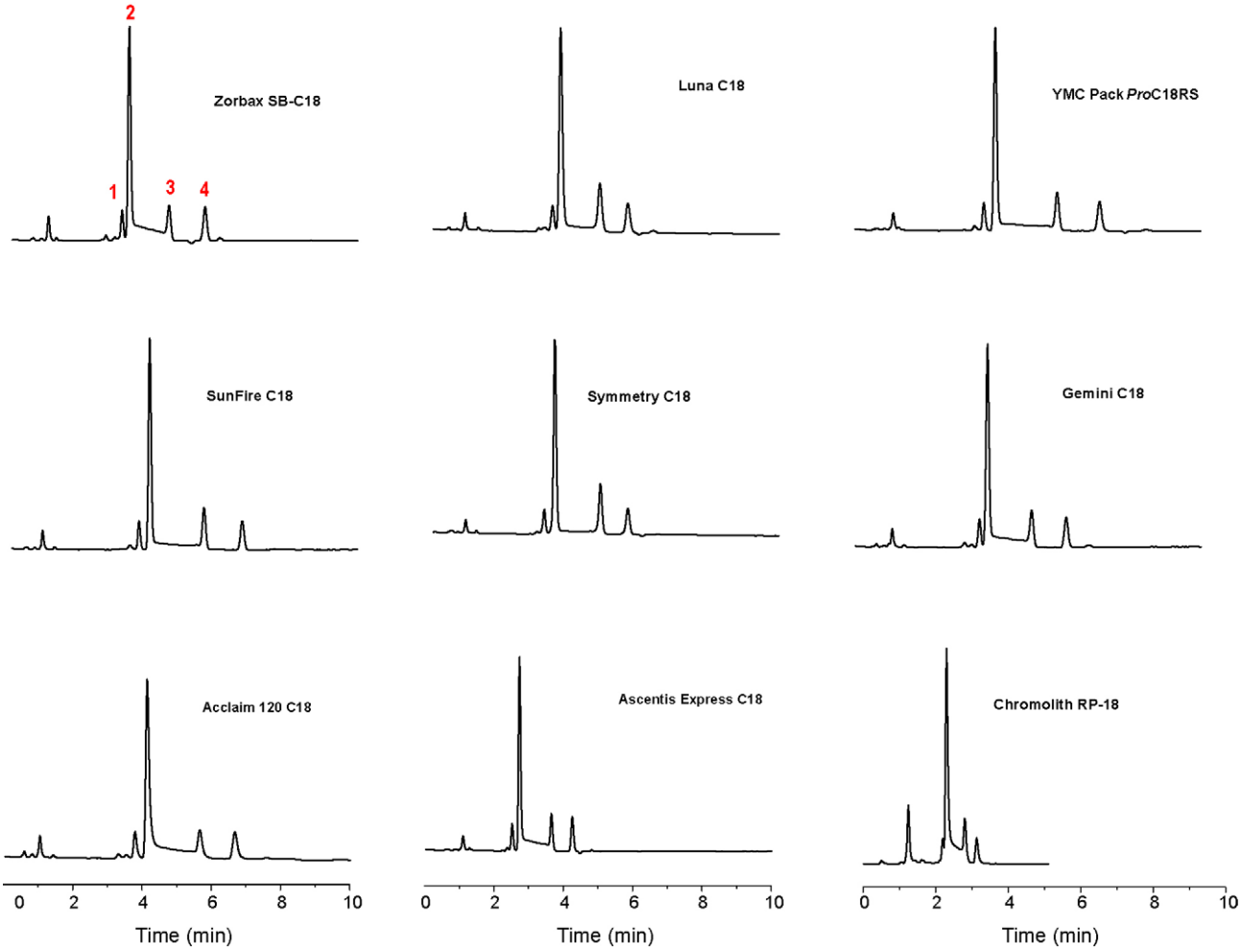

Fig. 3. Typical room temperature chromatograms obtained for a standard mixture of compounds **1** and **2** (containing **3** as impurity). Peak 1 corresponds to **3**, peak 2 to the **2**α-epimer, peak 3 to the **2**β-epimer, and peak 4 to **1**. Columns: Zorbax SB-C18, Luna C18, YMC-Pack *Pro*C18 RS, SunFire C18, Symmetry C18, Gemini C18, Acclaim 120 C18, Ascentis Express C18 (150 mm × 4.6 mm I.D.), and Chromolith RP-18 (100 mm × 4.6 mm I.D.); eluent: acetonitrile–water (60:40, v/v); flow-rate: 1.00 ml/min, T = 25 °C; UV detection at 210 nm.

Table 2
Room temperature chromatographic data for the tested commercial RP-C18 column[a]

Column	Dimension (mm)	ΔP (p.s.i.)	Peak 1			2 vs. 1		Peak 2			3 vs. 2		Peak 3			4 vs. 3		Peak 4		
			t_R min	k' [b]	A_s [c]	α [d]	R_s [e]	t_R min	k' [b]	A_s [c]	α [d]	R_s [e]	t_R min	k' [b]	A_s [c]	α [d]	R_s [e]	t_R min	k' [b]	A_s [c]
Zorbax SB-C18	150 × 4.6	570	3.21	1.17	0.94	1.13	1.48	3.42	1.32	1.06	1.62	6.92	4.57	2.13	1.04	1.35	5.33	5.61	2.87	1.00
Luna C18	150 × 4.6	920	3.47	1.14	1.00	1.14	1.38	3.71	1.30	1.16	1.55	5.61	4.84	2.02	1.02	1.26	3.48	5.64	2.54	1.38
YMC-Pack *Pro*C18 RS	150 × 4.6	1030	3.75	1.47	1.04	1.15	2.03	4.08	1.69	1.10	1.73	9.59	5.87	2.92	1.07	1.28	5.56	7.09	3.75	1.05
SunFire C18	150 × 4.6	1830	3.70	1.40	1.03	1.15	2.12	4.01	1.61	1.08	1.66	9.50	5.58	2.67	1.06	1.28	5.80	6.68	3.41	1.00
Symmetry C18	150 × 4.6	1480	3.24	1.19	1.11	1.18	2.07	3.55	1.41	0.99	1.66	7.90	4.86	2.34	0.92	1.24	4.16	5.65	2.90	0.94
	100 × 4.6	1250	2.28	1.19	1.09	1.18	1.63	2.48	1.40	1.12	1.68	6.61	3.40	2.35	1.07	1.25	3.63	3.96	2.93	1.09
	75 × 4.6	890	1.76	1.20	n.r. [f]	1.17	< 1	1.91	1.41	1.07	1.65	5.36	2.58	2.33	1.13	1.26	2.91	3.02	2.93	1.05
Gemini C18	150 × 4.6	1700	3.62	1.13	0.94	1.12	1.50	3.85	1.27	1.03	1.61	7.10	5.12	2.05	0.98	1.30	4.84	6.12	2.66	1.01
Acclaim 120 C18	150 × 4.6	1400	3.80	1.22	1.24	1.18	1.92	4.15	1.44	1.40	1.65	7.34	5.67	2.37	1.34	1.26	4.24	6.69	2.99	1.20
Ascentis Express C18	150 × 4.6	2300	2.53	0.83	1.01	1.19	1.80	2.74	0.99	1.14	1.72	7.54	3.66	1.70	1.11	1.27	4.52	4.26	2.16	1.09
Chromolith RP-18	100 × 4.6	190	2.20	0.47	n.r. [f]	1.17	< 1	2.30	0.55	1.42	1.65	4.18	2.81	0.91	1.42	1.26	2.49	3.14	1.15	1.42

[a] Eluent: acetonitrile–water = 60:40 (v/v); flow-rate: 1.00 ml/min; T = 25 °C; UV detection at 210 nm; $t_{0,\text{ext.}}$ = 0.15 min. Peak 1 = **3**; peak 2 = **2**α; peak 3 = **2**β; peak 4 = 1.
[b] k', retention factor = $(t_R - t_0)/t_{0,\text{corr.}} = (t_R - t_0)/(t_0 - t_{0,\text{extra column}})$.
[c] A_s: Asymmetry factor.
[d] α: selectivity factor.
[e] R_s: USP resolution.
[f] Not resolved.

antimalarial drugs [32]. In the monograph on *Artenimolum* or *Artenimol* (i.e., dihydroartemisinin) the method currently recommended is an HPLC assay based on the use of a stainless steel column (100 mm × 4.6 mm I.D.) packed with a reversed-phase C18 stationary phase (3.0 μm particle size). The mobile phase is acetonitrile–water 60:40 (v/v), delivered at a flow-rate of 0.6 ml/min and the detection system used is an ultraviolet spectrophotometer set at a wavelength of about 216 nm. The aim of the pharmacopoeial method is to quantitate dihydroartemisinin (**2**) in the presence of artemisinin (**1**) as related substance. The monograph does not provide for any other related substance. The final requirement is that "the test is not valid unless the relative retention of α-artenimol compared with artemisinin is about 0.6, and the resolution between the peaks is not less than 2.0. Measure the areas of the peak (twin-peak) responses and calculate the percentage content of $C_{15}H_{22}O_5$ (i.e., artemisinin) with reference to the dried substance".

Four main items raised when considering the above method: (i) the column temperature is not specified, (ii) no mention is made of the interconversion between the two epimers of **2**, which indeed occurs in the chromatographic time scale, (iii) the conditions are not very selective towards **3**, which is a ubiquitous contaminant of **2**, and (iv) signal-to-noise ratios in the presence of plateau zones are always smaller than in normal elution profiles; as a consequence, quantitation of species eventually eluting in the plateau would be negatively affected.

To overcome such shortcomings and try to address the four points, we investigated nine commercial RP-C18 columns (150 mm × 4.6 mm I.D.) with different morphological and physicochemical properties, such as specific surface areas (ranging from 150 to 500 $m^2\,g^{-1}$), particle sizes (from 2.7 to 5.0 μm), pore sizes (from 80 to 120 Å), carbon loads (from 2.00 to 3.76 $\mu mol\,m^{-2}$), and permeabilities (from 1.18 to 4.41 × 10^{-14} m^2). We also included in the study a monolithic column (100 mm × 4.6 mm I.D.). Details on the columns are collected in Table 1. On the nine columns we analyzed the standard mixture of compounds **1** and **2** (containing **3** as impurity), prepared as described in Section 2.4, under pharmacopoeial chromatographic conditions, and at different flow-rates. Since the column temperature was not specified, we performed the preliminary chromatographic runs by setting the temperature at 25 °C. In all cases, we found four chromatographic peaks with an invariant elution order, which were attributed as follows: peak 1 corresponds to **3**, peak 2 to **2**α, peak 3 to **2**β, and peak 4 to **1**. Typical chromatograms obtained on the tested columns are illustrated in Fig. 3. An interference regime (plateau) between the **2**α and **2**β resolved peaks was detected in all cases, and it is diagnostic of an interconversion process active between the **2**α (peak 2) and **2**β (peak 3) epimers during their chromatographic separation. Different peak shape deformations were observed, depending on the stationary phase considered. Chromatographic data for the tested commercial RP-C18 columns are presented in Table 2. As it can be observed, the investigated peaks were resolved under pharmacopoeial chromatographic conditions, all exhibiting a notable symmetrical shape (A_s < 1.42). Selectivity factors (α) between **3** and **2**α ranged from 1.12 to 1.19, whereas greater values were reached for the **2**β and **1** couple (α between 1.24 and 1.35). The highest selectivities were found for epimer couple **2**α and **2**β (α between 1.55 and 1.73), the most selective column being the YMC-Pack *Pro*C18 RS (α = 1.73), followed by the Ascentis Express C18 (α = 1.72). Finally, relative retention of **2**α (peak 2) compared with **1** (peak 4) was in good agreement with the pharmacopoeial requirements, ranging from 0.58 to 0.66 for the conventional particle-packed columns, reaching 0.73 for the monolithic column.

The main drawback of the method is that the presence of the visible plateau between the two dihydroartemisinin epimers is completely neglected. In addition, stationary phases may have a retarding or activating effect on the kinetics of the dynamic process involving stereolabile species during their passage through the chromatographic column. Therefore, it was necessary to investigate the epimerization process in the presence of the stationary phase.

3.2. Evaluation of stationary phases

Since the Pharmacopoeia monograph establishes quantification of dihydroartemisinin from the twin-peak area (i.e., the sum of α- and β-artenimol against that of artemisinin used as reference), it seemed relevant to evaluate to what extent the secondary

Table 3
Activation free energies and apparent rate constants for the interconversion process of **2**, obtained at T = 25 °C by computer simulation and comparison with the corresponding off-column data

Column	$K_{\alpha/\beta}$[a]	Interconversion process **2**α → **2**β			Interconversion process **2**α → **2**β				
		$^{app}\Delta G^{\#}$ (kcal mol^{-1})	$^{app}k_v$ (10^{-2} min^{-1})	CESP[b] (%)	$^{app}\Delta G^{\#}$ (kcal mol^{-1})	$^{app}k_v$ (10^{-2} min^{-1})	CESP[b] (%)	Plateau area[a] (%)	% error[c] $K_{\alpha/\beta}$
Symmetry C18[d]	3.1	22.1	2.30	−48.1	21.6	5.38	−62.4	9.2	−3.7
Symmetry C18[e]	3.1	22.0	2.82	−36.3	21.5	6.69	−53.2	5.8	−4.2
Symmetry C18[f]	3.3	22.0	2.81	−36.6	21.5	6.61	−53.8	5.0	2.1
Luna C18	3.3	21.9	3.52	−20.5	21.3	8.62	−39.7	11.2	1.7
SunFire C18	3.9	21.7	4.40	−0.7	21.2	10.1	−29.4	21.4	22.6
YMC-Pack *Pro*C18 RS	4.1	21.6	5.26	18.7	21.2	11.7	−18.2	22.5	29.1
Gemini C18	4.3	21.5	6.60	49.0	21.0	15.9	11.2	21.6	34.1
Acclaim 120 C18	4.8	21.4	7.90	78.3	20.9	18.5	29.4	24.3	50.2
Zorbax SB-C18	4.5	21.2	9.88	123.0	20.7	23.7	65.7	27.2	40.2
Ascentis Express C18	4.4	21.2	10.2	130.2	20.7	24.3	69.9	25.5	36.4
Chromolith RP-18	–	21.1	11.9	168.6	20.6	31.4	119.6	15.5	30.4
		$^{mob}K_{\alpha/\beta}$		$^{mob}\Delta G^{\#}$		$^{mob}k_v$		$^{mob}\Delta G^{\#}$	$^{mob}k_v$
Off-column[g]		3.2		21.7		4.43		21.0	14.3

[a] Calculated by peak areas integrated as depicted in Fig. 5.
[b] Catalytic effect of stationary phase: CESP = $[(^{app}k_v - {}^{mob}k_v)/{}^{mob}k_v] \times 100$.
[c] $[(K_{\alpha/\beta} - {}^{mob}K_{\alpha/\beta})/{}^{mob}K_{\alpha/\beta}] \times 100$.
[d] Column geometry: 150 mm × 4.6 mm I.D.
[e] Column geometry: 100 mm × 4.6 mm I.D.
[f] Column geometry: 75 mm × 4.6 mm I.D.
[g] Off-column data obtained at T = 25 °C.

equilibrium between **2**α and **2**β could impact the quantitation of **2**. We therefore performed a preliminary thermodynamic and kinetic study of the **2**α ⇄ **2**β epimerization process under pharmacopoeial conditions. We checked the equivalence of the UV absorption coefficients for **2**α and **2**β epimers at the operative wavelength by comparing chromatographic peak area ratios of **2**α and **2**β at 210 nm ($^{HPLC}K_{\alpha/\beta}$ = 3.5) with the corresponding ratios calculated by suitable integrated resonance signals selected within the ^{1}H-NMR spectra of **2**α and **2**β ($^{H\text{-}NMR}K_{\alpha/\beta}$ = 3.5) in the same solvent mixture (see Section 2.5 for details). Off-column epimerization of solid **2**β in mobile phase was performed by incubating the species into a thermostated reactor and monitoring the process by optimized cryo-HPLC conditions (*vide infra*). Equilibrium constant of the **2**α ⇄ **2**β process, $^{mob}K_{\alpha/\beta}$, and pseudo first-order rate constants for the interconversions of **2**α to **2**β, $^{mob}kv_{\alpha-\beta}$ and **2**β to **2**α, $^{mob}kv_{\beta-\alpha}$, were determined at T = 25 °C in mobile phase, and are collected in Table 3. As expected, the half-lives of both **2**α → **2**β and **2**β → **2**α processes, inferred by the related rate constants at 25 °C, matched the time scale of their separation, thus accounting for the presence of plateau zones between the corresponding chromatographic peaks. To evaluate the influence of the interconversion process on the chromatographic performance, we performed lineshape analysis (DHPLC simulations) of all the elution profiles in Fig. 3. As an example, Fig. 4 shows a comparison of experimental and simulated chromatograms, obtained for the YMC-Pack *Pro*C18 RS, Symmetry C18, and Chromolith RP-18 columns. As previously reported [36], rate constants of a given equilibrium determined by dynamic chromatography (the apparent rate constants k_1^{app} and k_{-1}^{app} related to the forward and backward reaction, respectively) are mean values weighted by the retention factors (k'_A and k'_B) of the processes occurring in both mobile (k_1^m and k_{-1}^m) and stationary phases (k_1^s and k_{-1}^s), according to Eqs. (1)–(2).

$$k_1^{app} = \frac{1}{1+k'_A}k_1^m + \frac{k'_A}{1+k'_A}k_1^s \quad (1)$$

$$k_{-1}^{app} = \frac{1}{1+k'_B}k_{-1}^m + \frac{k'_B}{1+k'_B}k_{-1}^s \quad (2)$$

where k'_A and k'_B are the retention factors of the first (A) and second (B) eluting species, respectively. If rate constants in mobile phase, i.e., k_1^m and k_{-1}^m are available from independent measurements, the rate constants in stationary phase, i.e., k_1^s and k_{-1}^s can be obtained as well by computer simulation. Therefore, within the input section of the program, we set rate constants in mobile phase (k_1^m and k_{-1}^m) as equal to those off-column measured for the **2**α → **2**β and **2**β → **2**α processes in the same media ($^{mob}kv_{\alpha-\beta}$ and $^{mob}kv_{\beta-\alpha}$), so that their ratio k_1^m/k_{-1}^m is always consistent with the experimentally measured thermodynamic ratio ($K_{\alpha/\beta}$ = 3.2 in acetonitrile–water 60:40, v/v). Table 3 reports the apparent pseudo-first order rate constants for **2**α → **2**β and **2**β → **2**α conversions ($^{app}kv_{\alpha-\beta}$ and $^{app}kv_{\beta-\alpha}$, respectively) and the related activation free energies ($^{app}\Delta G^{\#}_{\alpha-\beta}$ and $^{app}\Delta G^{\#}_{\beta-\alpha}$), calculated by the Eyring Equation. Also inserted in Table 3 are: (i) the percentage amounts of the interconverted fractions of **2**, responsible for the plateau zones (ratios between plateau zones area and total **2** area obtained by integrating from peak 2 to peak 3), and (ii) the $K_{\alpha/\beta}$ constants calculated by peaks 3 and 2 area ratio, integrated in presence of the plateau zone (see Fig. 5 for details on the integration mode used).

By comparison of $^{mob}kv_{\alpha-\beta}$ and $^{mob}kv_{\beta-\alpha}$ with the corresponding $^{app}kv_{\alpha-\beta}$ and $^{app}kv_{\beta-\alpha}$ values, we were able to characterize each column for its ability to promote or inhibit epimerization of **2**.

We defined the Catalytic Effect of Stationary Phases (CESP) as the percentage increasing (positive) or decreasing (negative) of the epimerization rate constant, with respect to the analogous value measured in mobile phase (see Table 3). On this basis, three columns (Symmetry C18, Luna C18, and SunFire C18) of the nine investigated were shown to reduce the **2**α ⇄ **2**β interconversion rate, whereas the others increased the rate of the dynamic process, with the exception of the YMC-Pack *Pro*C18 RS column, which indeed did not show any appreciable effect. According to these findings, columns with negative CESP values (see Table 3) provided chromatograms with smaller plateau area, that is, a smaller error in quantitation of **2** can be made when using such columns. In

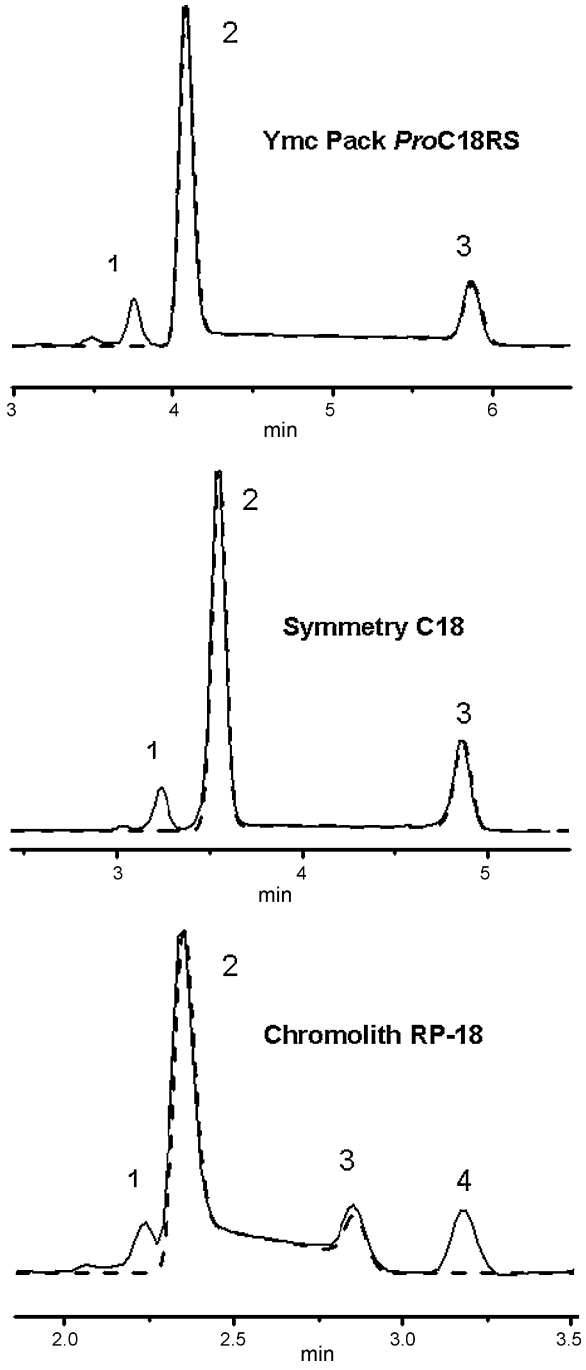

Fig. 4. Comparison of experimental (solid line) and simulated (dotted line) chromatograms. Columns: YMC-Pack *Pro*C18 RS (150 mm × 4.6 mm I.D.), Symmetry C18 (150 mm × 4.6 mm I.D.), and Chromolith RP-18 (100 mm × 4.6 mm I.D.); eluent: acetonitrile–water (60:40, v/v); flow-rate: 1.00 ml/min, T = 25 °C; UV detection at 210 nm. Simulations were performed by use of the lab-made computer program Auto DHPLC y2k [34].

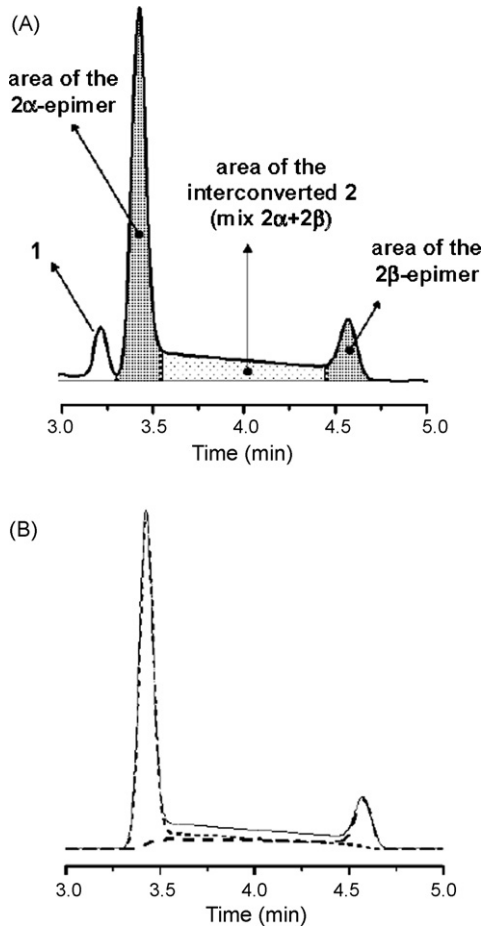

Fig. 5. (A) Schematic representation of the integration mode used for the calculation of **2**α and **2**β-epimers area. (B) Computer simulated profiles of **2**α (dotted line), **2**β (dashed line), and of the mixture **2**α + **2**β (solid line).

particular, for the Symmetry C18 and Luna C18 columns, such an error (plateau area ≤ 11%) is about the half of that found for the other columns (>21%). A further and definitive confirmation of the convenience in the use of the Symmetry C18 and/or Luna C18 columns for their inhibiting effect on epimerization derived from the more precision in the $K_{\alpha/\beta}$ constant measurement. Such columns led to acceptable error ranges (<4%), whereas in the other cases the error raised to 22%, up to 50%. On the basis of the above considerations, the Symmetry C18 column was selected to perform a more in-depth investigation.

3.3. Investigation of the selected Symmetry C18 column

The Symmetry C18 column was tested in three different column geometries, i.e., 150, 100, and 75 mm × 4.6 mm I.D. As easily predictable, the less the column length, the less is the staying time of **2**α and **2**β epimers inside the separation device. Therefore, lower plateau areas were obtained when reducing the column length (see Table 3), with comparable selectivity, but with lower efficiency and resolution (see Table 2). Typical room temperature chromatograms achieved on the Symmetry C18 columns are depicted in Fig. 6.

The up-to-now findings clearly demonstrated the role of the stationary phase (i.e., type and column length) in minimizing quantitation errors of **2**. However, we decided to investigate the influence of column temperature on the epimerization process, which is always relevant when considering sterically labile compounds.

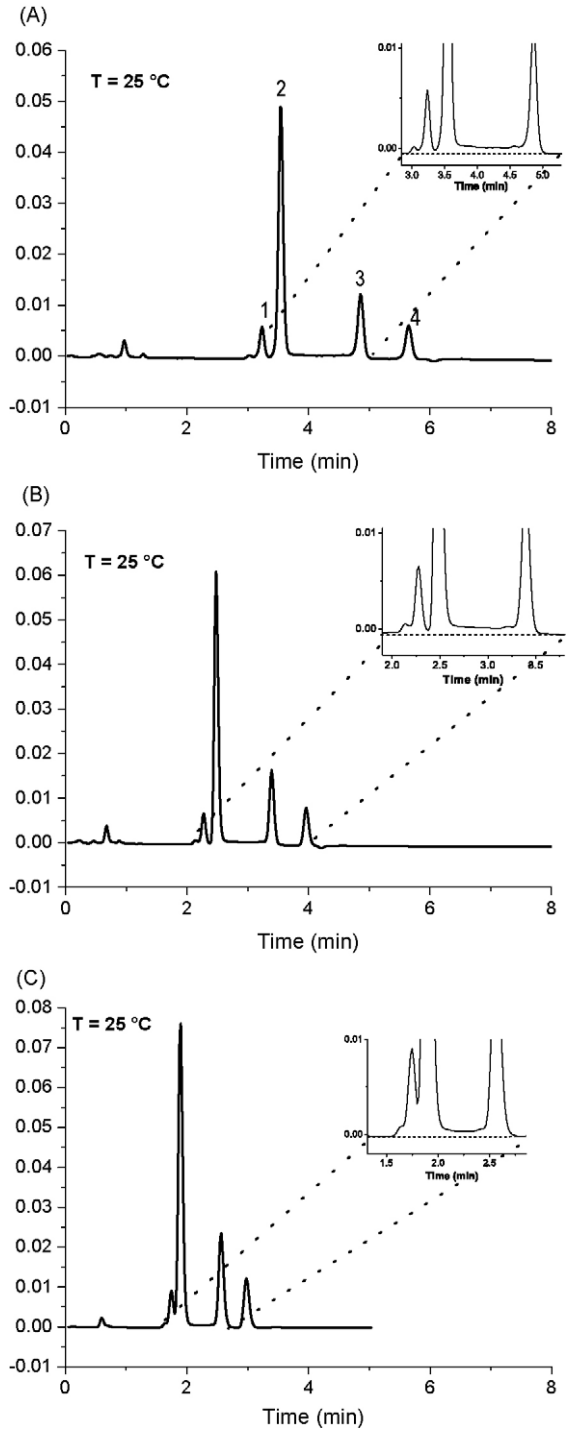

Fig. 6. Typical room temperature chromatograms obtained on the Symmetry C18 columns family for a standard mixture of compounds **1** and **2** (containing **3** as impurity). Peak 1 corresponds to **3**, peak 2 to the **2**α-epimer, peak 3 to the **2**β-epimer, and peak 4 to **1**. Columns geometry: A: 150 mm × 4.6 mm I.D.; B: 100 mm × 4.6 mm I.D.; C: 75 mm × 4.6 mm I.D.; eluent: acetonitrile–water (60:40, v/v); flow-rate: 1.00 ml/min, T = 25 °C; UV detection at 210 nm.

3.4. Diastereoselective dynamic HPLC (DHPLC)

Variable temperature separations were performed on the Symmetry C18 column, in the geometry recommended by the Pharmacopoeial monograph (i.e., 100 mm × 4.6 mm I.D.). The temperature range was of 40–0 °C. Since plateau zones were easily

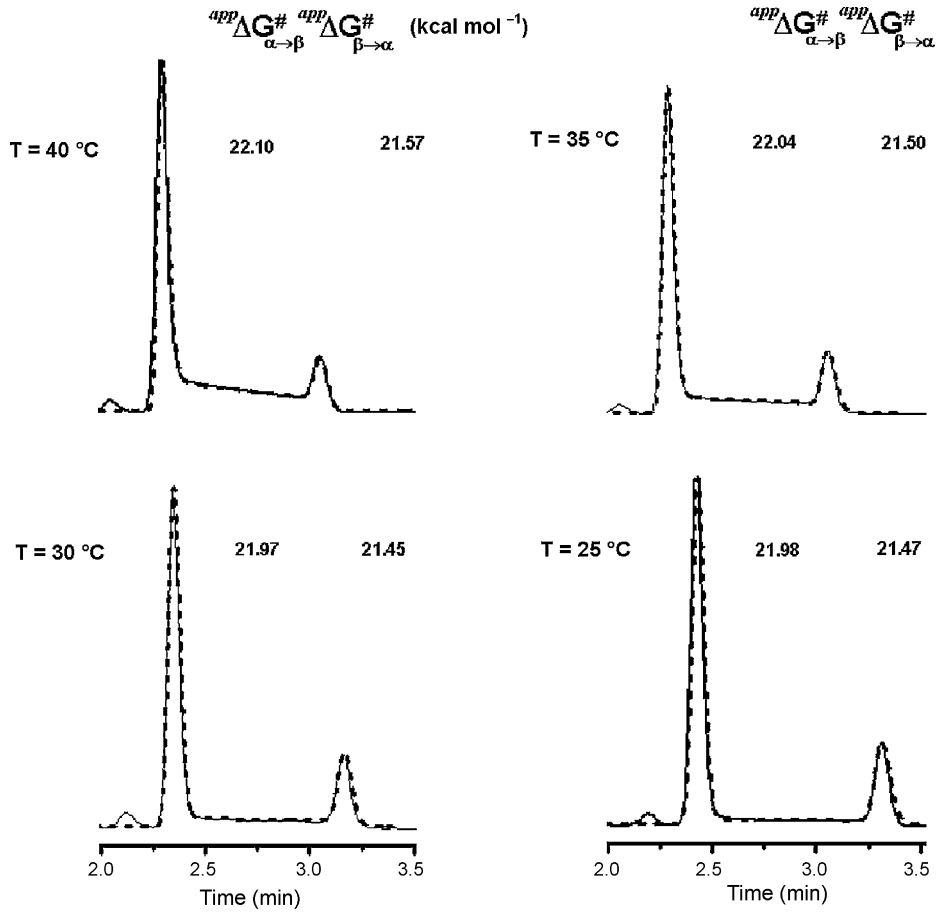

Fig. 7. Variable temperature chromatographic profiles obtained on the Symmetry C18 column (100 mm × 4.6 mm I.D.). Solid line: experimental chromatograms (eluent: acetonitrile–water 60:40 v/v, flow-rate: 1.00 ml/min, UV detection at 210 nm). Dotted line: computer simulated profiles obtained with the measured free energy activation barriers for the on-column epimerization process.

visible only at $T > 20\,^{\circ}C$, simulations of the chromatograms registered from 40 to 25 °C were performed by using the classical stochastic model, as implemented within the Auto DHPLC y2k program [34]. Fig. 7 shows the superimposed experimental and simulated chromatographic profiles with the measured activation free energies. van't Hoff analyses of the obtained data were also carried out to evaluate the enthalpic and entropic contributions to the epimerization barrier, and the related plots are depicted in Fig. 8. As judged by the obtained results, just a very small contribution to $\Delta G^{\#}_{\alpha-\beta}$ and $\Delta G^{\#}_{\beta-\alpha}$ is due to entropy ($\Delta S^{\#}$ values < 10 u.e.). This suggests that a monomolecular process must be involved in the rate-determining step, reasonably, the ring opening of either the protonated or deprotonated α- or β-hemiacetalic form of **2**, generated in a previous reversible step by reaction with an acid or a base, respectively. Such kinetic pathway would be in agreement to what already reported [10].

3.5. Cryo-HPLC on the selected Symmetry C18 columns family

Low-temperature separations were performed on the Symmetry C18 column, in the three different column lengths, i.e., 150, 100, and 75 mm × 4.6 mm I.D., and at $T = 0$, 5, and 10 °C. Lower plateau

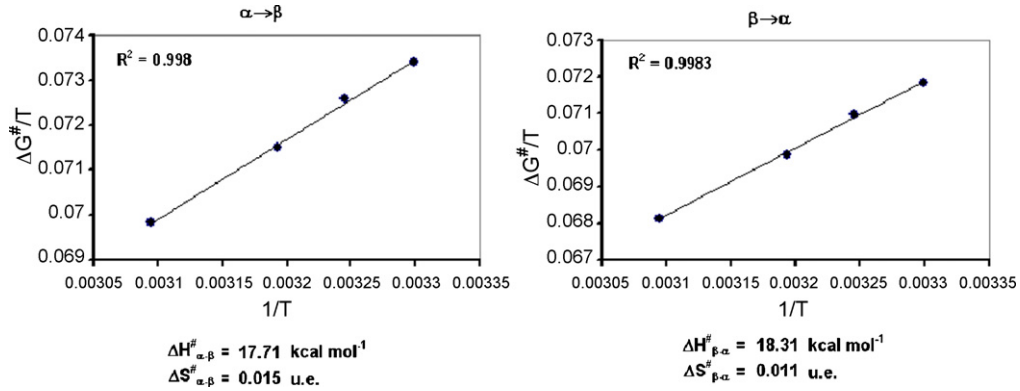

Fig. 8. van't Hoff plots obtained by DHPLC for the **2**α ⇄ **2**β interconversion. Column: Symmetry C18 column (100 mm × 4.6 mm I.D.).

Table 4
Low-temperature chromatographic data for the Symmetry RP-C18 columns[a]

Column	Dimension (mm)	T (°C)	Peak 1			2 *vs* 1		]Peak 2			3 *vs* 2		Peak 3			4 *vs* 3		Peak 4		
			t_R (min)	k'[b]	A_s[c]	α[d]	R_s[e]	t_R (min)	k'[b]	A_s[c]	α[d]	R_s[e]	t_R (min)	k'[b]	A_s[c]	α[d]	R_s[e]	t_R (min)	k'[b]	A_s[c]
Symmetry C18	150 × 4.6 (t_0 = 2.60 min)	0	5.92	1.41	1.07	1.15	1.98	6.41	1.62	1.10	1.70	8.91	9.09	2.76	1.04	1.32	5.74	11.18	3.65	1.04
		5	5.81	1.37	0.99	1.14	2.05	6.28	1.57	0.99	1.70	9.35	8.89	2.67	0.92	1.31	5.85	10.88	3.52	0.93
		10	5.67	1.31	0.93	1.15	2.06	6.14	1.51	0.96	1.70	9.21	8.65	2.57	0.90	1.30	5.50	10.45	3.34	0.50
	100 × 4.6 (t_0 = 1.87 min)	0	4.15	1.41	1.13	1.13	1.07	4.44	1.59	1.14	1.73	6.42	6.34	2.76	1.14	1.35	4.47	7.90	3.72	1.15
		5	4.07	1.36	1.30	1.13	1.17	4.36	1.54	1.14	1.73	6.51	6.20	2.67	1.14	1.35	4.41	7.72	3.61	1.14
		10	3.96	1.29	1.18	1.15	1.36	4.28	1.49	1.18	1.72	7.14	6.03	2.57	1.13	1.30	4.67	7.30	3.35	1.13
	75 × 4.6 (t_0 = 1.46 min)	0	3.20	1.43	n.r.[f]	1.12	<1	3.40	1.60	n.r.[f]	1.71	5.29	4.77	2.73	1.19	1.35	3.73	5.91	3.68	1.20
		5	3.13	1.38	n.r.[f]	1.12	<1	3.34	1.55	n.r.[f]	1.72	5.36	4.69	2.67	1.18	1.33	3.64	5.77	3.56	1.19
		10	3.06	1.32	n.r.[f]	1.14	1.03	3.28	1.50	1.12	1.72	5.48	4.58	2.58	1.15	1.31	3.53	5.56	3.39	1.16

[a] Eluent: acetonitrile/water = 60/40 (v/v); flow-rate 0.60 ml/min; UV detection at 210 nm; $t_{0,ext.}$ = 0.25 min. Peak 1 = **3**; peak 2 = **2**α; peak 3 = **2**β; peak 4 = **1**.
[b] k', Retention factor = $(t_R - t_0)/t_{0,corr.} = (t_R - t_0)/(t_0 - t_{0,extra\ column})$.
[c] A_s: Asymmetry factor.
[d] α: Selectivity factor.
[e] R_s: USP resolution.
[f] Not resolved.

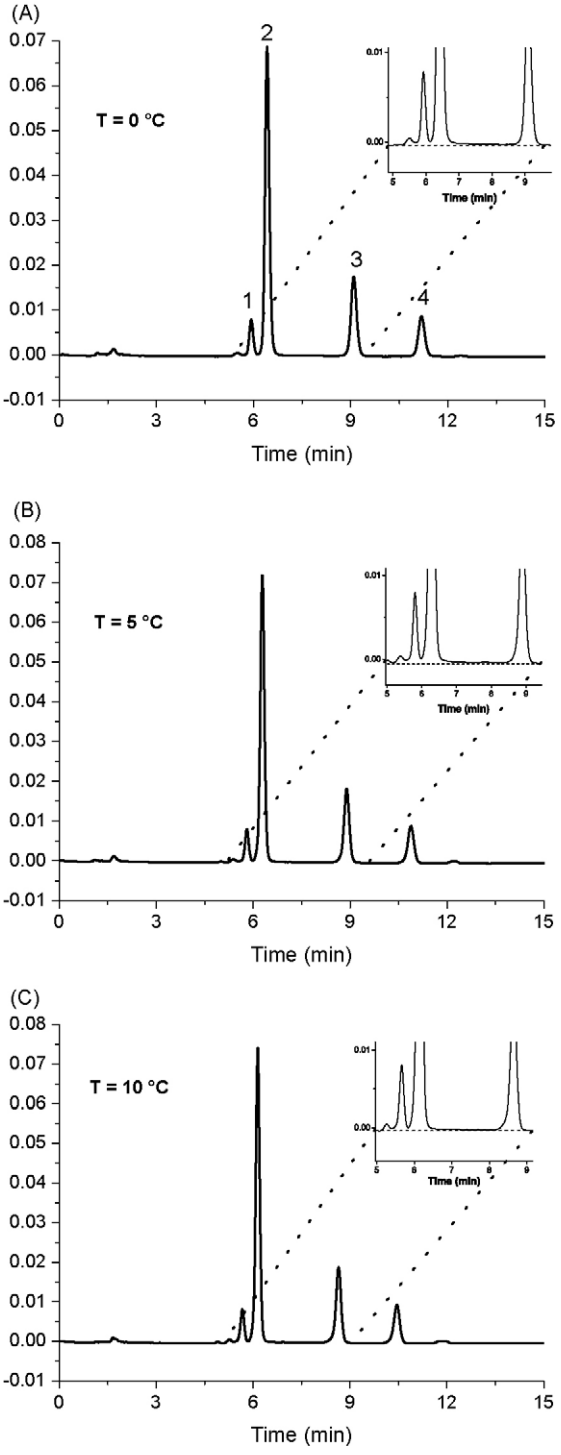

Fig. 9. Cryo-HPLC/UV profiles obtained on the Symmetry C18 column (150 mm × 4.6 mm I.D.) for a standard mixture of compounds **1** and **2** (containing **3** as impurity). Peak 1 corresponds to **3**, peak 2 to the **2**α-epimer, peak 3 to the **2**β-epimer, and peak 4 to **1**. Eluent: acetonitrile–water 60:40 (v/v); flow-rate: 0.60 ml/min, T = 0 °C (A), 5 °C (B), and 10 °C (C); UV detection at 210 nm.

areas were obtained when decreasing from T = 25 to 0 °C (data not shown), but slightly lower efficiency and resolution were found, as judged by the chromatographic data presented in Table 4. Resolution factors (R_S) between **3** and **2**α slightly decreased from 2.07 at T = 25 °C (see Table 2) to 1.98–2.06 at T = 0–10 °C (Table 4) on the

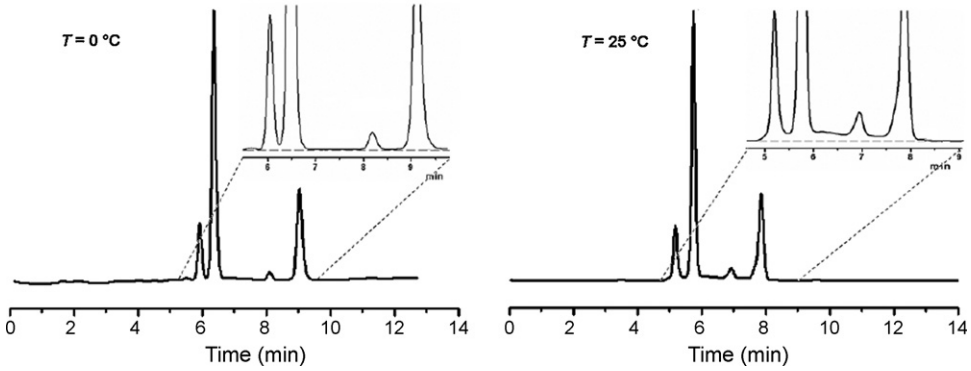

Fig. 10. Chromatogram profiles obtained at $T = 0\,^{\circ}C$ (left) and $T = 25\,^{\circ}C$ (right) for a methanol solution of **2** heated in an oven at 90 °C for 4 h: an unknown impurity is eluting in the plateau zone. Column: Symmetry C18 column (100 mm × 4.6 mm I.D.); eluent: acetonitrile–water (60:40, v/v); flow-rate: 0.60 ml/min; UV detection at 210 nm.

150 mm Symmetry C18 column, whereas for the 100 mm column such decreasing is more relevant (from 1.63 to 1.07–1.36, respectively). A baseline resolution between **3** and **2**α was achieved only on the 150 mm Symmetry C18 column. A direct comparison of the chromatograms obtained on such column at the three column temperatures further supports the convenience in the use of the 150 mm Symmetry C18 column under cryo-HPLC conditions (Fig. 9) On the basis of the epimerization rate constants extrapolated at $T < 25\,^{\circ}C$, we calculated a marginal plateau area (<2%) only close to $T = 0\,^{\circ}C$ (Fig. 10, left). We are currently testing buffered mobile phases to given pHs aimed at minimizing on-column epimerization without drastically decreasing column temperature. No relevant influence of flow-rates on the chromatographic performances was observed when checked on the Symmetry C18 column (75 mm × 4.6 mm I.D.), at $T = 10\,^{\circ}C$ (data not shown).

A final consideration on the Pharmacopoeian method can be made in the case of chemical impurities eventually eluting in the plateau zone (see Fig. 10, right): quantitation of **2** in such cases could be difficult to obtain and usually overestimated.

4. Conclusions

A systematic investigation was made on the influence of chromatographic conditions (stationary phase and column temperature) on the simultaneous reversed-phase HPLC determination of artemisinin (**1**), α-dihydroartemisinin (**2**α), β-dihydroartemisinin (**2**β), and a thermal decomposition product of **2** (diketoaldehyde **3**), considering for the first time the on-column epimerization process of **2**. Nine commercial RP-C18 columns with different pore size, surface area, carbon load and permeability were evaluated starting from the International Pharmacopoeia monograph on dihydroartemisinin, and compared on the basis of their stationary phase effect towards the interconversion between **2**α and **2**β. Computer simulation was employed to gain insight on the Catalytic Effect of the Stationary Phase (CESP). Activation free energies of the process, obtained by computer simulation of the experimentally obtained elution profiles, showed that the Symmetry C18 column among the nine analyzed has an inhibiting effect on epimerization ($\Delta G^{\#} = 22.1$ for **2**α → **2**β and 21.6 kcal mol^{-1} for the backward process). The column was selected for the development of a cryo-HPLC method aimed at minimizing on-column interconversion. On the basis of the epimerization rate constants extrapolated at $T < 25\,^{\circ}C$, we calculated a marginal plateau area (<2%) only close to $T = 0\,^{\circ}C$ for the 150 mm × 4.6 column geometry. In another related paper, buffered mobile phases to given pHs will be tested to minimize on-column epimerization without drastically decreasing column temperature. UPLC will be investigated as well as an alternative technique to yield fast analysis without compromising the efficiency of separation.

Acknowledgements

Financial support from FIRB, Research program: Ricerca e Sviluppo del Farmaco (CHEM-PROFARMA-NET), grant no. RBPR05NWWC_003 is acknowledged.

The authors gratefully acknowledge Giovanna Cancelliere (Sapienza Università di Roma, Italy) for helpful assistance in the manuscript editing, and Andrea Mazzanti (Università di Bologna, Italy) for performing NMR spectra of dihydroartemisinin.

References

[1] D.L. Klayman, Science 228 (1985) 1049.
[2] P.M. O'Neill, Expert Opin. Invest. Drugs 14 (2005) 1117.
[3] P.M. O'Neill, G.H. Posner, J. Med. Chem. 47 (2004) 2945.
[4] L. Ying, P. Yu, Y. Chen, L. Li, Y. Gai, D. Wang, Y. Zheng, Chin. Sci. Bull. 24 (1979) 667.
[5] China Cooperative Research Group on qinghaosu, its derivatives as antimalarials, J. Tradit. Chin. Med. 2 (1982) 9.
[6] A.K. Pathak, D.C. Jain, R.P. Sharma, Indian J. Chem., Sect. B: Org. Chem. Incl. Med. Chem. 34 (1995) 992.
[7] R.K. Haynes, H.W. Chan, M.K. Cheung, S.T. Chung, W.L. Lam, H.W. Tsang, A. Voerste, I.D. Williams, Eur. J. Org. Chem. (2003) 2098.
[8] X. Luo, H.J.C. Yeh, A. Brossi, J.L. Flipper-Anderson, R. Gillardi, Helv. Chim. Acta 67 (1984) 1515.
[9] R.K. Haynes, H.W. Chan, M.K. Cheung, W.L. Lam, M.K. Soo, H.W. Tsang, A. Voerste, I.D. Williams, Eur. J. Org. Chem. (2002) 113.
[10] R.K. Haynes, Curr. Med. Chem. 6 (2006) 509.
[11] Z.M. Zhou, J.C. Anders, H. Chung, A.D. Theoharides, J. Chromatogr. 414 (1987) 77.
[12] V. Melendez, J.O. Peggins, T.G. Brewer, A.D. Theoharides, J. Pharm. Sci. 80 (1991) 132.
[13] V. Navaratnam, S.M. Mansor, L.K. Chin, M.N. Mordi, M. Asokan, N.K. Nair, J. Chromatogr. B 669 (1995) 289.
[14] J. Karbwang, K. Na-Bangchang, P. Molunto, V. Banmairuroi, K. Congpuong, J. Chromatogr. B 690 (1997) 259.
[15] N. Sandrenan, A. Sioufi, J. Godbillon, C. Netterb, M. Danker, C. van Valkenburg, J. Chromatogr. B 691 (1997) 145.
[16] V. Navaratnam, M.N. Mordi, S.M. Mansor, J. Chromatogr. B 692 (1997) 157.
[17] C.-S. Lai, N.K. Nair, S.M. Mansor, P.L. Olliaro, V. Navaratnam, J. Chromatogr. B 857 (2007) 308.
[18] K.T. Batty, T.M.E. Davies, L.T. Thu, T.Q. Binh, T.K. Anh, K.F. Ilett, J. Chromatogr. B 677 (1996) 345.
[19] K.T. Batty, K.F. Ilett, T.M.E. Davis, J. Pharm. Pharmacol. 48 (1996) 22.
[20] B.M. Kotecka, K.H. Rieckmann, T.M.E. Davis, K.T. Batty, K.F. Ilett, Acta Trop. 87 (2003) 371.
[21] B.A. Avery, K.K. Venkatesh, M.A. Avery, J. Chromatogr. B 730 (1999) 71.
[22] D. Ortelli, S. Rudaz, E. Cognard, J.-L. Veuthey, Chromatographia 52 (2000) 445.
[23] C. Souppart, N. Gauducheau, N. Sandrenan, F. Richard, J. Chromatogr. B 774 (2002) 195.
[24] S. Sabarinath, M. Rajanikanth, K.P. Madhusudanan, R.C. Gupta, J. Mass Spectrom. 38 (2003) 732.
[25] M. Rajanikanth, K.P. Madhusudanan, R.C. Gupta, Biomed. Chromatogr. 17 (2003) 440.
[26] H. Naik, D.J. Murry, L.E. Kirsch, L. Fleckenstein, J. Chromatogr. B 816 (2005) 233.
[27] K.T. Batty, K.F. Ilett, T.M.E. Davis, Br. J. Clin. Pharmacol. 57 (2004) 529.

[28] Z. Shishan, Chromatographia 22 (1986) 77.
[29] N. Liu, L. Yang, Z. Zhang, Chin. J. Pharm. Anal. 22 (2002) 303.
[30] A.J. Lin, A.D. Theoharides, D.L. Klayman, Tetrahedron 42 (1986) 2181.
[31] L. Dhooghe, S. Van Miert, H. Jansen, A. Vlietinck, L. Pieters, Pharmazie 62 (2007) 12.
[32] International Pharmacopoeia, fourth ed., Monographs for Antimalarial Drugs, WHO Press, Geneva, 2006, pp. 215–218.
[33] (a) K. Stott, J. Keeler, Q.N. Van, A.J. Shaka, J. Magn. Reson. 125 (1997) 302;
(b) T. Parella, P. Adell, F. Sánchez-Ferrando, A. Virgili, Magn. Reson. Chem. 36 (1998) 245.
[34] (a) F. Gasparrini, L. Lunazzi, A. Mazzanti, M. Pierini, K.M. Pieyrusiewicz, C. Villani, J. Am. Chem. Soc. 122 (2000) 4776;
(b) C. Dell'Erba, F. Gasparrini, S. Grilli, L. Lunazzi, A. Mazzanti, M. Novi, M. Pierini, C. Tavani, C. Villani, J. Org. Chem. 67 (2002) 1663;
(c) A. Dalla Cort, F. Gasparrini, L. Lunazzi, L. Mandolini, A. Mazzanti, C. Pasquini, M. Pierini, R. Rompietti, L. Schiaffino, J. Org. Chem. 70 (2005) 8877;
(d) F. Gasparrini, S. Grilli, R. Leardini, L. Lunazzi, A. Mazzanti, D. Nanni, M. Pierini, M. Pinamonti, J. Org. Chem. 67 (2002) 3089;
(e) R. Cirilli, R. Ferretti, F. La Torre, D. Secci, A. Bolasco, S. Carradori, M. Pierini, J. Chromatogr. A 1172 (2007) 160.
[35] (a) M. Jung, QCPE Bull. 12 (1992) 52;
(b) O. Trapp, V. Schurig, Comput. Chem. 25 (2001) 187.
[36] (a) J.C. Giddings, J. Chromatogr. 3 (1960) 443;
(b) R. Kramer, J. Chromatogr. 107 (1975) 241;
(c) V. Schurig, W. Burkle, J. Am. Chem. Soc. 104 (1982) 7573;
(d) W. Burkle, H. Karfunkel, V. Schurig, J. Chromatogr. 288 (1984) 1;
(e) J. Veciana, M.I. Crespo, Angew. Chem. Int. Ed. Engl. 30 (1991) 74;
(f) O. Trapp, G. Schoetz, V. Schurig, Chirality 13 (2001) 403;
(g) O. Trapp, Anal. Chem. 78 (2006) 189;
(h) J. Oxelbark, S. Allenmark, J. Chem. Soc. Perkin Trans. 28 (1999) 1587;
(i) C. Wolf, Chem. Soc. Rev. 34 (2005) 595;
(j) K. Cabrera, M. Jung, M. Fluck, V. Schurig, J. Chromatogr. A 731 (1996) 315;
(k) R. Kiesswetter, F. Brandl, N. Kastner-Pustet, A. Mannschreck, Chirality 15 (2003) S40.